Research Communication

Astrakurkurone, a Sesquiterpenoid from Wild Edible Mushroom, Targets Liver Cancer Cells by Modulating Bcl-2 Family Proteins

Adhiraj Dasgupta[1]
Dhritiman Dey[2]
Dipanjan Ghosh[2]
Tapan Kumar Lai[3]
Nattamai Bhuvanesh[4]
Sandip Dolui[5]
Ravichandiran Velayutham[2]
Krishnendu Acharya[1]*

[1]Molecular and Applied Mycology and Plant Pathology Laboratory, Department of Botany, University of Calcutta, Kolkata, WB, India
[2]Department of Natural Products, National Institute of Pharmaceutical Education and Research (NIPER) Kolkata, Kolkata, WB, India
[3]Department of Chemistry, Vidyasagar Evening College, Kolkata, WB, India
[4]Department of Chemistry, Texas A&M University, College Station, TX, USA
[5]Structural Biology and Bioinformatics Division, Indian Institute of Chemical Biology, Council of Scientific and Industrial Research, Kolkata, WB, India

Abstract

Induction of apoptosis is the target of choice for modern chemotherapeutic treatment of cancer, where lack of potent "target-specific" drugs has led to extensive research on anticancer compounds from natural sources. In our study, we have used astrakurkurone, a triterpene isolated from wild edible mushroom, *Astraeus hygrometricus*. We have discussed the structure and stability of astrakurkurone employing single-crystal X-ray crystallography and studied its potential apoptogenicity in hepatocellular carcinoma (HCC) cells. Our experiments reveal that it is cytotoxic against the HCC cell lines (Hep 3B and Hep G2) at significantly low doses. Further investigations indicated that astrakurkurone acts by inducing apoptosis in the cells, disrupting mitochondrial membrane potential and inducing the expression of Bcl-2 family proteins, for example, Bax, and the downstream effector caspases 3 and 9. A molecular docking study also predicted direct interactions of the drug with antiapoptotic proteins Bcl-2 and Bcl-xL. Thus, astrakurkurone could become a valuable addition to the conventional repertoire of future anticancer drugs. © 2019 IUBMB Life, 71(7):992–1002, 2019

Keywords: apoptosis; mitochondrial apoptosis; hepatocellular carcinoma; B-cell lymphoma-2 (Bcl-2) family; B-cell lymphoma-2 (Bcl-2); mitochondrial membrane potential; astrakurkurone

INTRODUCTION

Cancer is a well-recognized global health problem responsible for approximately 7.6 million deaths per annum (13% of all deaths) worldwide, which is expected to rise to 13.1 million by 2030 (1). Despite remarkable progress in the field of cancer research, both developing and developed countries are in the grip of this deadly disease, and still there is a need to discover and develop anticancer therapeutic agents. Apart from genetic causes, smoking, heavy metal pollution, and sedentary life style, coupled with increased affinity to low-fiber fast food, also contribute toward a leap in the incidences of cancer (1).

Decades of medical research have given us several treatment strategies for cancer, among which chemotherapy is the major line of choice. Chemotherapy usually targets cellular apoptosis, a pathway intrinsic to all cells. A chemotherapeutic agent can activate apoptosis in several ways, for example, by binding to cell death receptors onto the membrane or by modulating the Bcl-2 (B-cell lymphoma-2) family proteins at the intracellular level, both resulting in the release of cytochrome *c* in the cytosol followed by activation of caspases. The Bcl-2 family includes both proapoptotic and antiapoptotic proteins, and an intricate balance between these proapoptotic and antiapoptotic signals determines the fate of the cells. As the Bcl-2 family of proteins reside upstream of irreversible

Additional Supporting Information may be found in the online version of this article.

Abbreviations: *AO, acridine orange; Bcl-2, B-cell lymphoma-2; BH, Bcl homology domain; DAPI, 4′,6-diamidino-2-phenylindole; DCFDA, 2′,7′-dichlorofluorescein diacetate; DiOC6, 3,3′-dihexyloxacarbocyanine iodide; EB, ethidium bromide; FITC, fluorescein isothiocyanate; HCC, hepatocellular carcinoma; MMP, mitochondrial membrane potential; ROS, reactive oxygen species*

Volume 71, Number 7, July 2019, Pages 992–1002

*Address correspondence to: Krishnendu Acharya, Department of Botany, Molecular and Applied Mycology and Plant Pathology Laboratory, University of Calcutta, 35, Ballygunge Circular Road, Kolkata 700019, West Bengal, India. Tel: (091) 8013167310. E-mail: krish_paper@yahoo.com

Received 12 January 2019; Accepted 26 March 2019
DOI 10.1002/iub.2047
Published online 12 April 2019 in Wiley Online Library (wileyonlinelibrary.com)

cellular damage and focus much of their efforts at the level of mitochondria, they play a pivotal role in deciding whether a cell will live or die (2). In the absence of death signals, considerable amounts of proapoptotic and antiapoptotic members of the Bcl-2 family localize subcellularly in different compartments. A substantial fraction of the proapoptotic members localizes to the cytosol prior to a death signal (3). Following a death signal, the proapoptotic members undergo conformational changes that enable them to target and integrate into membranes, especially the mitochondrial outer membrane, altering the pro–anti ratio of Bcl-2 proteins in the cytosol, thereby allowing downstream protein modifications or dimerization converting inactive conformers to active ones and inducing cell death (4).

Modern-day chemotherapy may be the first choice of treatment, but it comes with its own disadvantages that include untargeted tissue damage and multidrug resistance (5). This often results in severe side effects and deterioration in the quality of life of patients. Thus, in the recent times, the demand for more effective and less toxic cancer chemopreventers mainly from natural sources has increased dramatically (6). Among the natural sources that are being sought, mushrooms have come up with immense potential. Mushrooms are rich in proteins, carbohydrates, and unsaturated fatty acids and low in fat content. Apart from the traditional food value, mushrooms are also considered as sources for next-generation pharmaceuticals and nutraceuticals because they contain a wide range of biologically active phenols, flavones, terpenes, and many more active components. These molecules, in raw extracts, additively and synergistically act against several human ailments (7). Several mushroom species, their extracts and isolated compounds, have been screened for anticancer activity, and many have yielded promising results. Approximately 200 species of mushrooms have been reported to exhibit antitumor activity (8), and many of these mushroom-derived compounds have already been put to clinical use (9–11). This vastly unexplored source of pharmacologically active compounds promises to add to the repertoire of adjuvant therapeutics in the days to come.

Astraeus hygrometricus is a wild edible mushroom commonly found in the laterite forests near the roots of *Shorea robusta* trees. Its ethnomedicinal role has been documented in preventing several diseases (12). We have recently isolated a novel triterpene, astrakurkurone, from *A. hygrometricus* and partially characterized it (13). Our previous research revealed that this triterpene possesses antileishmanial (14, 15) and anticandidal activities (13). In this study, we report X-ray crystallographic analysis of a single crystal of astrakurkurone. We also report its effectiveness against hepatocellular carcinoma (HCC) cell lines Hep 3B and Hep G2 and try to predict a possible pathway to its anticancer activity.

EXPERIMENTAL PROCEDURES

Crystallography

Single crystals of astrakurkurone were developed by slow evaporation of the material solution in 20% EtOH in chloroform. The crystallographic data for astrakurkurone were collected on a Bruker GADDS X-ray (three-circle) diffractometer at 110 K with Cu-Kα1 (λ = 1.5418 Å) radiation using a graphite monochromator. The goniometer was controlled using the FRAMBO software v.4.1.05 (16). Data analysis was performed by the program APEX2 (17). SADABS (18) was employed to correct the data for absorption effects. OLEX2 was employed for the structure plots (19).

The sample was optically centered with the aid of a video camera such that no translations were observed as the crystal was rotated through all positions. The detector was set at 5.0 cm from the crystal sample. 180 data frames were taken at widths of 0.5°. These reflections were used to determine the unit cell using Cell_Now (20). The unit cell was verified by examination of the *hkl* overlays on several frames of data. No super-cell or erroneous reflections were observed. The integration method employed a three-dimensional profiling algorithm, and all data were corrected for Lorentz and polarization factors as well as for crystal decay effects. Finally, the data were merged and scaled to produce a suitable data set. SADABS (18) was employed to correct the data for absorption effects.

Cell Culture

The liver cancer cell lines Hep 3B and Hep G2 were purchased from the cell line repository at the National Centre for Cell Science (NCCS), Pune, India, and maintained in Dulbecco's Modified Eagle Medium (MP Biomedicals, Santa Ana, CA, USA) with 10% fetal bovine serum (Gibco, Waltham, MA, USA), 100 U/mL penicillin, and 100 μg/mL streptomycin (Gibco, Waltham, MA, USA). They were incubated in a humidified incubator with 5% CO_2 at 37 °C until 80–90% confluence. The cells were trypsinized with trypsin–EDTA (Gibco, Waltham, MA, USA) and used for experiments.

Astrakurkurone was dissolved in dimethyl sulfoxide (DMSO) (Merck, Kenilworth, NJ, USA) to obtain a stock concentration of 20 mM, which was further diluted for experiments. At no point of our experiments did the concentration of DMSO exceed 1% during treatment. All experiments were performed on cells treated with astrakurkurone for 24 h.

In Vitro Cytotoxicity Assay

Hep 3B and Hep G2 cells were seeded in a 96-well microtiter plate and incubated for 24 h. The cells were treated with different concentrations of astrakurkurone (20–220 μM). After 24 h, 10 μL of the WST-1 reagent (TaKaRa, Kusatsu, Japan) was added to each well and incubated for 2 h. Absorbance was measured using a microplate reader as per manufacturer's protocol. The reduction in absorbance was used as an indicator of cell death and to determine the LD_{50} value.

Cell Migration Assay

The cells were seeded in 6-well plates and grown to confluence. The cells were treated with half LD_{50} concentrations of astrakurkurone, and scratches were made on the plate using a microtip. The cells were visualized for migration at 0 h and after 24 h and photographed.

Fluorescence Microscopy and Apoptosis Detection by Acridine Orange/Ethidium Bromide Staining

The cells treated with different concentrations of astrakurkurone were stained with a mixture of acridine orange (AO, 5 mg/mL) and ethidium bromide (EB, 3 mg/mL) and visualized under a fluorescence microscope (FLoid Imaging Station, Life Technologies, Waltham, MA, USA). The live cells were stained green due to the uptake of AO while the dead cells took up EB preferentially, producing a brilliant orange fluorescence.

To study changes in nuclear morphology, treated cells were washed with phosphate-buffered saline (PBS), fixed with 4% paraformaldehyde in PBS for 10 minutes, again washed with PBS, and finally stained with 4′,6-diamidino-2-phenylindole (DAPI) (1 μg/mL in PBS) for 15 minutes. The cells were then examined under a fluorescence microscope for nuclear deformities.

Flow Cytometric Analysis of Cellular Apoptosis and Cell Cycles

Astrakurkurone-treated HCC cells were harvested and examined for apoptosis using the fluorescein isothiocyanate (FITC)-Annexin V/propidium iodide (PI) staining kit (BioLegend, San Diego, CA, USA) following the manufacturer's protocol. The harvested cells were washed with PBS and stained with FITC-Annexin V using Annexin V binding buffer for 30 minutes. PI solution was added to the cell suspension and studied for apoptosis.

In another experiment, to examine the cell cycle status of the treated cells, the harvested cells were fixed with 70% ethanol overnight. The fixed cells were centrifuged at 1000 rpm for 3 minutes and the supernatant was discarded. The cells were then washed with PBS and suspended in a buffer containing 50 μg/mL PI (21). The cells were incubated for 10 minutes and subjected to flow cytometry.

Flow Cytometric and Microscopic Analysis of Intracellular ROS

Healthy Hep 3B and Hep G2 cells were suspended in serum-free media, treated with varied concentrations of astrakurkurone, and incubated for 1 h. 5 μM DCFDA (2′,7′-dichlorofluorescein diacetate) was added to each set, incubated at 37° C for 15 minutes, and examined by flow cytometry. Healthy HCC cells grown to 70–80% confluence were substituted with serum-free media and treated with different concentrations of astrakurkurone and 5 μM DCFDA in combination. The cells were studied under a fluorescence microscope for the detection of intracellular reactive oxygen species (ROS) after an hour-long incubation at 37° C.

Flow Cytometric Analysis of Mitochondrial Membrane Potential

$DiOC_6$ (3,3′-dihexyloxacarbocyanine iodide) is a cell-permeant green-fluorescent lipophilic dye, selective for the mitochondria of live cells, at low concentrations. Harvested cells were washed and resuspended in PBS. 0.1 μM $DiOC_6$ was added to each sample and examined by flow cytometry.

RNA Isolation and Semiquantitative Reverse Transcriptase Polymerase Chain Reaction

Total cellular RNA of treated and untreated cells was isolated using the TRIzol reagent (MP Biomedicals, Santa Ana, CA, USA) following the manufacturer's protocol. RNA was quantified, and equal quantities of RNA were used to synthesize cDNA by reverse transcriptase polymerase chain reaction. The produced cDNA was used to study the expression of apoptosis-related genes bax and Bcl-2. GAPDH was used as the internal control. The specific primer sequences were selected from the published literature, and are shown in Table S7.

Western Blot Analysis

To prepare the whole cell lysate, the treated cells were harvested by trypsinization and suspended in radioimmunoprecipitation assay buffer (25 mM Tris–HCl, pH 7.6, 150 mM NaCl, 1% NP-40, 1% sodium deoxycholate, and 0.1% sodium dodecyl sulfate [SDS]) supplemented with protease inhibitors. The lysate was centrifuged at 13000 rpm for 30 minutes and the supernatant was collected. Total protein content was measured using the Bradford reagent (Abcam, Cambridge, UK).

Equal amounts of protein from the control set and each of the treated sets were separated by SDS-PAGE (10%) and transferred onto a polyvinylidene fluoride membrane. The membrane was blocked with 5% bovine serum albumin and incubated overnight with the primary antibodies of bax, Bcl-2, cleaved caspase 3, cleaved caspase 9 (GeneTex Inc., Alton Pkwy Irvine, CA, USA), and GAPDH (BioBharati LifeScience, Kolkata, India). The membrane was then washed with PBS-T and incubated with horseradish peroxidase-conjugated secondary antibody for 1 h. Protein expression was studied by chemiluminescence in a ChemiDoc Gel Imaging System (Bio-Rad, Hercules, CA, USA) using the horseradish peroxidase substrate (Thermo Fisher Scientific, Waltham, MA, USA). Antibodies were stripped off the membrane using Restore Western Blot Stripping Buffer (Thermo Fisher Scientific, Waltham, MA, USA) before every subsequent analysis after the first one.

Binding Analysis by Molecular Docking

Molecular docking studies were carried out to further understand and characterize the interaction of astrakurkurone with Bcl-2. Astrakurkurone was drawn in gauss view and optimized at the B3LYP/6-311 + G (d,p) level using the Gaussian 09 program. The optimized ligand structure was docked into the protein using the AutoDock version 4.2. AutoDockTools 1.5.4 was used to set the polar hydrogen and rotatable bonds, and also to add the Gasteiger charge. The protein box surrounded in the grid box has a dimension of 126 Å × 126 × Å × 126 Å with a grid spacing of 0.375 Å. The Lamarckian genetic algorithm was used to generate the protein–ligand conformation. The docking was carried out with the following parameters: number of runs, 100; population size, 150; number of evaluations, 2,500,000; and the number of generations, 27,000. Cluster analysis was carried out with a root mean square deviation tolerance of 2 Å. The output was rendered by the PyMOL molecular viewer and MGLTools.

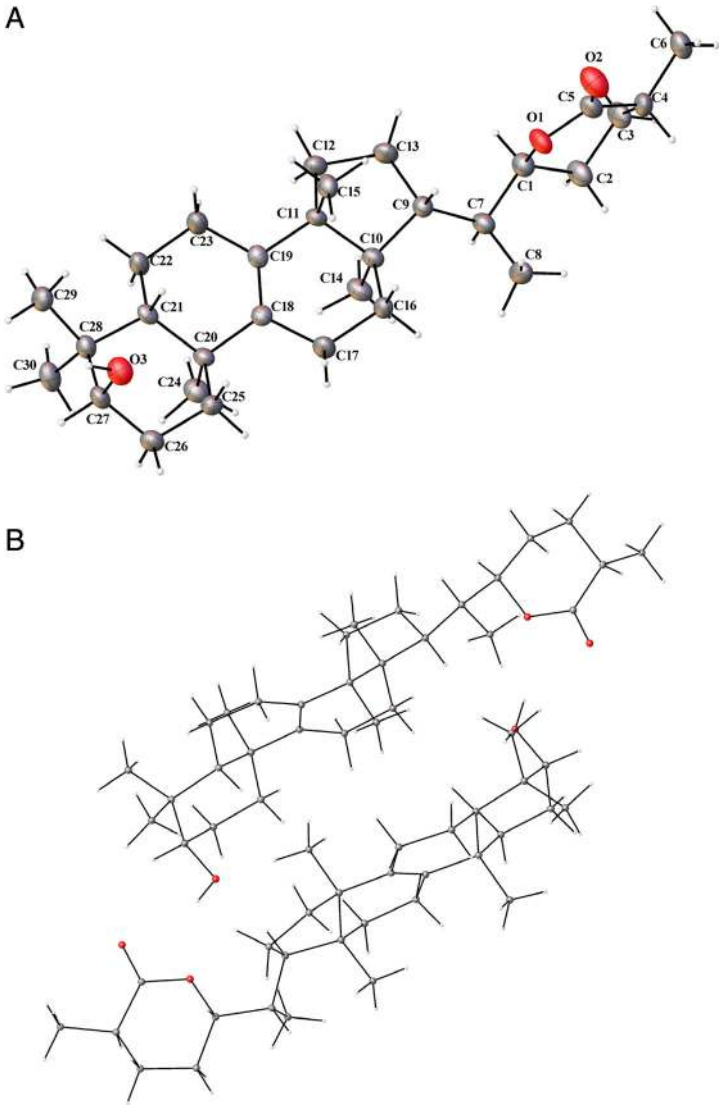

FIG 1 *(A) ORTEP representation of astrakurkurone. (B) Representative packing of two molecules of astrakurkurone in the crystal structure.*

Statistical Analysis

All data are presented as the mean ± SD of "n" independent measurements as indicated in the corresponding figure legends. Statistical comparisons between treated and untreated control groups were calculated using Student's *t* test. A value of $P < 0.05$ was considered significant.

RESULTS

Crystallographic Structure of Astrakurkurone

Astrakurkurone (TLB_150506_G) crystallizes in the $P2_1$ space group with $Z = 4$ and $Z' = 2$. The packing characteristics revealed, along expected lines, that the C(3)-OH of one molecule is hydrogen bonded to both the ring oxygen and the carbonyl oxygen of another molecule. An ORTEP diagram of the crystal structure (clarified thermal ellipsoids of a single molecule) is given in Fig. 1A and the representative packing of two molecules of the compound is given in Fig. 1B. A summary of crystal parameters is presented in Table 1. Detailed crystal information for astrakurkurone (TLB_150506_G) has been presented in Tables S1–S6. The crystallographic data have been deposited in the CCDC vide number 1831282.

TABLE 1 *Crystal data and structural refinement for TLB_150506_G*

Identification code	tplai
Empirical formula	C30 H48 O3
Formula weight	456.68
Temperature	110.15 K
Wavelength	1.54178 Å
Crystal system	Monoclinic
Space group	P 1 21 1
Unit cell dimensions	*a* = 13.4261(5) Å = 90°.□ *b* = 7.2851(3) Å = □ 102.490 (2)°. *c* = 27.9342(11) Å = 90°.□
Volume	2,667.59(18) Å^3
Z	4
Density (calculated)	1.137 Mg/m^3
Absorption coefficient	0.546 mm^{-1}
F(000)	1,008
Crystal size	0.37 × 0.06 × 0.04 mm^3
Theta range for data collection	3.241 to 60.848°
Index ranges	?<=h<=?, ?<=k<=?, ?<=l<=?
Reflections collected	?
Independent reflections	7,364 [*R*(int) = ?]
Completeness to theta = 67.679°	80.0%
Absorption correction	Semiempirical from equivalents
Max. and min. transmission	0.752 and 0.624
Refinement method	Full-matrix least-squares on F^2
Data/restraints/parameters	7,364/1/612
Goodness of fit on F^2	1.117
Final *R* indices [*I*>2sigma(*I*)]	R1 = 0.0508, wR2 = 0.1372
R indices (all data)	R1 = 0.0574, wR2 = 0.1495
Absolute structure parameter	0.1(2)
Extinction coefficient	0.0047(6)
Largest diff. peak and hole	0.392 and −0.252 e.Å^{-3}

Astrakurkurone Induces Cell Death and Reduces Cellular Migration of Liver Cancer Cells

WST-1 assay helped us to evaluate cell death at different concentrations of the drug and calculate its LD_{50} value, which was found to be 58.8 μM and 122 μM for Hep 3B and Hep G2, respectively (Fig. 2A,B). Comparative treatment of astrakurkurone on a normal liver cell line (Chang liver) showed no untargeted cytotoxicity even at the highest dose of 250 μM. The cells were also treated with a known anticancer drug doxorubicin for 24 hours. The LD_{50} value was found to be 4 μM for Hep 3B and 9 μM for Hep G2. The results are shown in Fig. S1A,B.

To further contrast between live and dead cells visually, dual staining with AO and EB was performed where the live cells fluoresce green due to AO uptake, while the dead cells glow orange for EB permeating selectively into dead cells. In our experiment, it could be visually confirmed that astrakurkurone induced cell death in HCC cells (Fig. 2C). Cell migration assays indicated that astrakurkurone reduced the migration of the liver cancer cells (Fig. 3) at half LD_{50} concentrations of 29 μM for Hep 3B and 61 μM for Hep G2.

Astrakurkurone Leads to Cell Cycle Arrest and Concomitant Apoptotic Induction in Liver Cancer Cells

The astrakurkurone-treated and untreated Hep 3B and Hep G2 cells were stained with PI and analyzed for anomalies in the cell cycle. Our results showed astrakurkurone-induced cell cycle arrest at the sub-G_0/G_1 phase in both Hep3B (35% at 40 μM dose) and Hep G2 (21% at 150 μM dose). At these concentrations, the cell population at sub-G_0 phase, indicative of apoptotic cells was found to increase significantly in comparison to untreated controls (Fig. 4B).

Alterations in DNA caused by several factors affect the nucleus and ultimately the entire cell leading to compromised function of the organ and organism. Thus, we wanted to assess the nuclear morphology of astrakurkurone-treated and untreated Hep 3B and Hep G2 cells using DAPI staining and fluorescence microscopy. We found that in comparison to the untreated controls, the nuclei of the treated cells (40 μM for Hep 3B and 150 μM for Hep G2) appeared shrunk, with pronounced blebbing, and these deformities could be observed after an incubation period of 24 h (Fig. 4A).

Various literature studies and preclinical and clinical evidence suggest that the key to regressing tumors and elimination of abnormal premalignant cells is the induction of apoptosis. In the current study, to confirm and quantify astrakurkurone-induced apoptosis, Annexin V/PI dual staining experiments were performed employing flow cytometry. Our experimental data (Fig. 5A) indicated that after exposure to 40 μM and 150 μM doses for 24 h, about 45% of Hep 3B cells and 90% of Hep G2 cells were in the apoptotic phases (early: Annexin V+ and late: Annexin V/PI+ phase cells taken together).

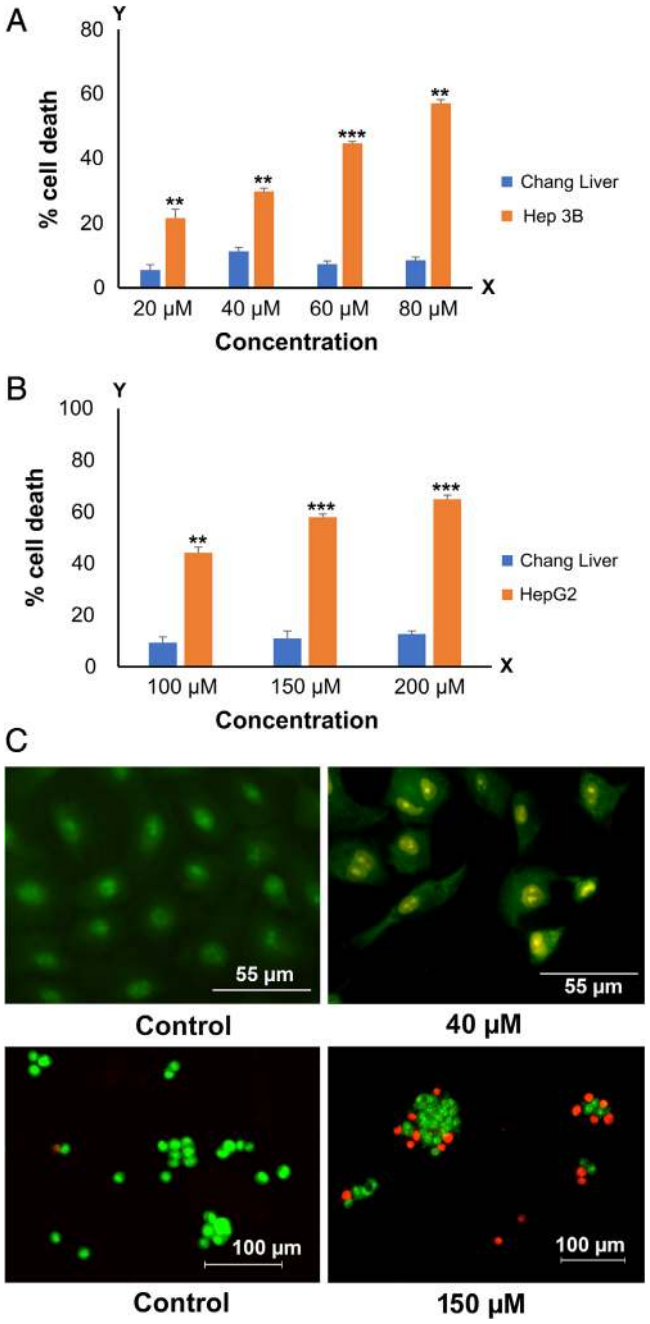

FIG 2

*Astrakurkurone-induced cytotoxicity in (A) Hep 3B cells and (B) Hep G2 cells. Chang liver cells were taken as normal liver cells after 24 h. Data are presented as mean ± SEM and are representative of three independent experiments. *P < 0.05; **P < 0.01; ***P < 0.001. (C) Cell death imaging by acridine orange and ethidium bromide dual staining as pictured after 24 h for Hep 3B (upper panel) and Hep G2 (lower panel) cells. Images taken under 20X magnification, representing the best of the replicates (n = 3).*

Astrakurkurone Is a Major MMP-Modulating Agent and Accentuates ROS Generation in Liver Cancer Cells

The cells in our study were coincubated with astrakurkurone and DCFDA, a fluorescent probe for ROS, and analyzed by flow cytometry. Our results suggest that the drug did induce ROS generation in the treated HCC cells, and that it is an early event. A substantial amount of ROS was detected as early as within

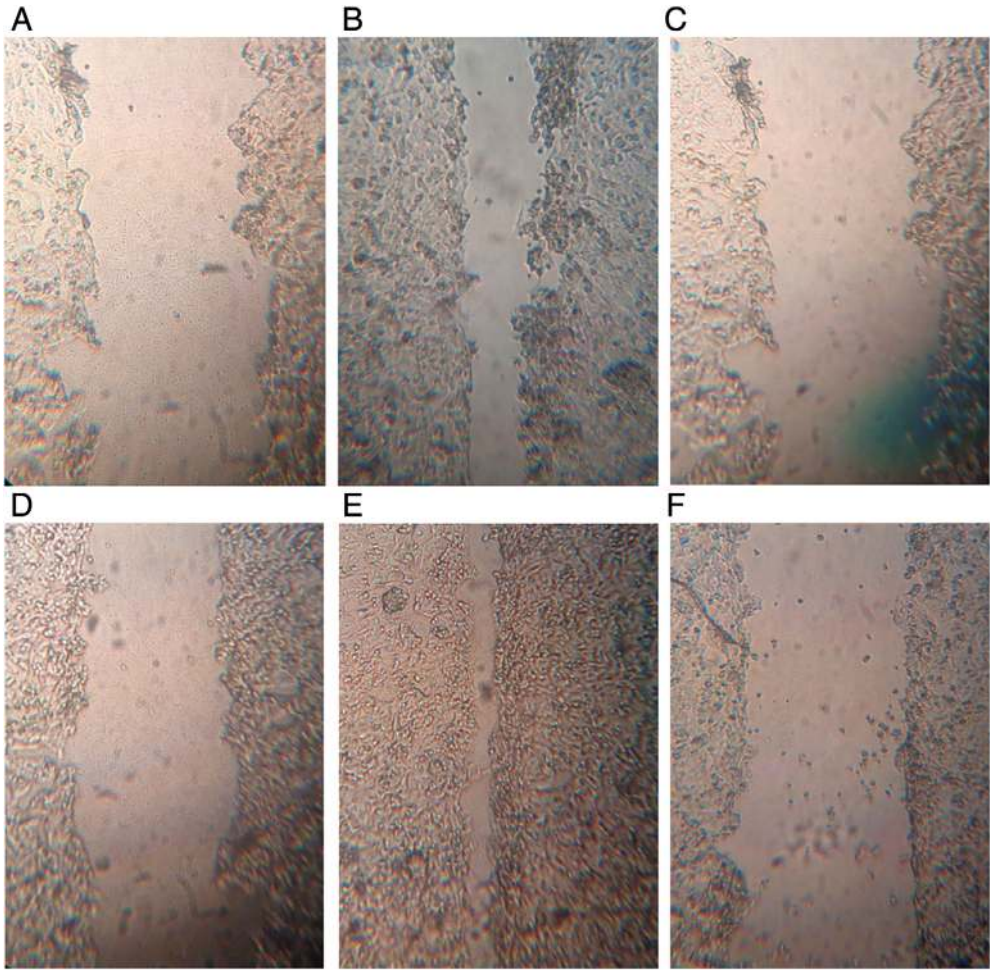

FIG 3 *Cell migration assay. (A) Untreated control Hep 3B cells at 0 h, (B) untreated control Hep 3B cells at 24 h, (C) Hep 3B cells treated with 29 μM astrakurkurone at 24 h, (D) untreated control Hep G2 cells at 0 h, (E) untreated control Hep G2 cells at 24 h, and (F) Hep G2 cells treated with 61 μM astrakurkurone at 24 h. Images taken under 5X magnification, representing the best of the replicates (n = 3).*

1 h of incubation as indicated by the peak shift in Hep 3B and Hep G2 (Fig. 6A-I,B-I, respectively).

We stained the HCC cells with a mitochondria-specific fluorescent probe $DiOC_6$ and analyzed them by flow cytometry. 3,3′-Dihexyloxacarbocyanine iodide ($DiOC_6$) is a cell-permeant, green-fluorescent, lipophilic dye that accumulates in mitochondria due to their large negative membrane potential and can be applied to monitor the mitochondrial membrane potential (MMP) using flow cytometric detection (22). A marked decrease in the fluorescence intensity of $DiOC_6$ was observed in the treated cells (40 μM for Hep 3B and 150 μM for Hep G2, Fig. 6A-II,B-II, respectively), indicating that astrakurkurone may have induced mitochondrial membrane depolarization leading to MMP disruption.

Astrakurkurone/BCL-2 Interaction Dictates the Predominant Interactions Between Antiapoptotic and Proapoptotic BCL-2 Family Proteins in the Liver Cancer Cells

Morphological and flow cytometric analysis of apoptosis in our study indicated that astrakurkurone might act by activating the intrinsic pathway of apoptosis. Gene expression studies clearly indicated a dose-dependent increase (20–80 μM for Hep3B; 50–200 μM for HepG2) in the mRNA expression of Bax. Bcl-2, however, was found to be downregulated compared to untreated controls (Fig. 5B-I,B-II). These findings corroborated with Western blot analysis where similar results were found at the protein levels from whole cell lysates of both cell lines. Further analysis of downstream effector caspases showed a dose-dependent increase in cleaved caspases 3 and 9 (Fig. 5C-I,C-II). The protein expression was normalized against GAPDH, and the relative protein expression for Hep3B and HepG2 has been indicated in Fig. S2A and S2B, respectively.

Molecular docking analysis by AutoDock 4.2 showed that astrakurkurone did bind inside the grooves of Bcl-xL and Bcl-2 (crystal structures of Bcl-xL PDB ID: 4QVF and Bcl-2 PDB ID: 2O2F were obtained from the Protein Data Bank). Figure 7A,C shows the lowest energy-binding pose is obtained by the molecular docking of astrakurkurone with Bcl-xL and Bcl-2 in a partial surface view. The lanostane moiety of astrakurkurone was placed

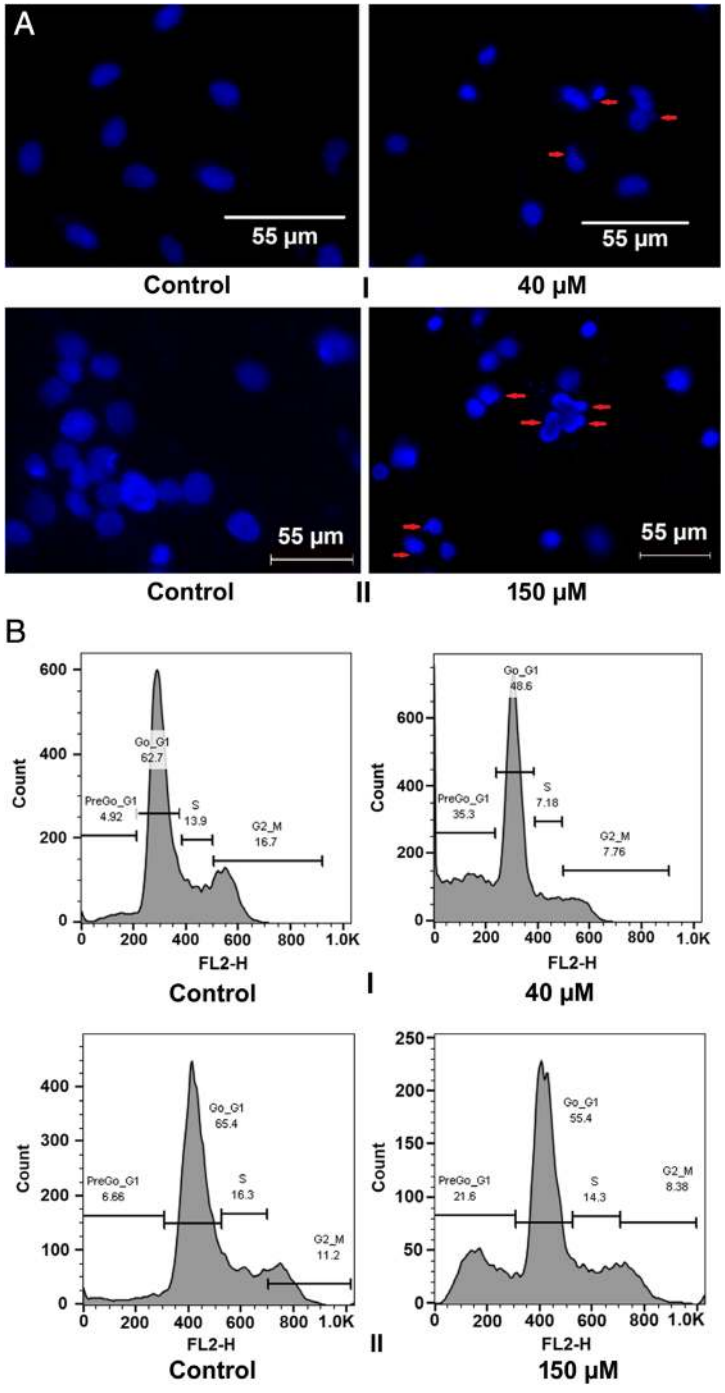

FIG 4

(A) Nuclear deformities in hepatocellular carcinoma (HCC) cells after 24 h treatment with astrakurkurone. I) Hep 3B cells and II) Hep G2 cells. Images taken under 20X magnification, representing the best of the replicates (n = 3). (B) Cell cycle analysis of PI-stained HCC cells showing an increase in apoptotic cell population after 24 h treatment with astrakurkurone: (I) Hep 3B cells and (II) Hep G2 cells. Data are expressed as mean ± SEM (n = 3), $P < 0.05$.

very close to the hydrophobic pocket (BH3 domain) of Bcl-xL interacting at Phe-97, Tyr-101, Ala-104, Phe-105, Val-126, and Phe-146. Similar amino acids interact with Bim at Leu-94 and Ile-97 (Fig. 7A,B). The pyran-2-one group of astrakurkurone was found in a different position, and it forms a hydrogen bond with His-113 of human Bcl-xL (Fig. 7B). The theoretical binding was energetically most favorable with a binding energy of –9.45 kcal/mol. Apart from these, the hydrophobic and hydrogen bond interactions are also predicted to play a significant role in the complex formation inside the binding pocket of Bcl-xL. In the case of Bcl-2, the pyran-2-one moiety of astrakurkurone lies near the human Bcl-2 residue Arg-104 (Fig. 7C,D). The pyran-2-one moiety interacted inside the binding pocket formed by Bcl-2 residues Ala-97, Phe-101, and Val-145. The lanostane moiety was observed in the hydrophobic pocket of Phe-109, Met-112, Val-130, Leu-134, and Ala-146. The binding (theoretical) was energetically most favorable with a binding energy of –9.34 kcal/mol. Upon interaction with Bcl-xL, the hydrophobic bonds are predicted to be involved in the complex formation inside the binding pocket of Bcl-2.

DISCUSSION

Liver cancer is the third major cause of cancer-related deaths worldwide. It is often detected late, rendering conventional chemotherapy, radiotherapy, or immunotherapy practically challenging (23). Pharmaceutical therapies are designed to activate cytotoxicity pathways in tumor cells, while maintaining some selectivity to minimize destruction of normal tissue (24). In our study, we evaluated the anticancer effects of our drug candidate astrakurkurone on two major HCC cells Hep 3B and Hep G2. Even though a few compounds have been isolated from mushrooms, not many have been structurally characterized in depth (25). Crystallographic analysis demonstrated a well-defined crystal structure of astrakurkurone, which was used for our downstream experiments. Astrakurkurone crystals showed significant cytotoxicity against the above-mentioned cell lines at significantly low doses, which showed no toxicity on normal liver cells (Chang liver). Astrakurkurone also showed a promising result in inducing cell cycle arrest at the sub-G0/G1 phase and arresting cellular migration in adherent cultures, thereby posing to be a possible therapeutic in line for inhibiting proliferation of liver cancer cells.

The major hallmark of human cancers is to evade the cell death signals (26), and this increases the importance of newly designed drugs that are targeted to activate the cell death machinery (27). Cell death by apoptosis is ATP dependent and is characterized by cell shrinkage, chromatin condensation, nuclear fragmentation, and activation of a family of cysteine-containing, aspartate-directed proteases called caspases (28). Even though cell death by apoptosis is characterized by DNA fragmentation, the appearance of a DNA ladder is not entirely conclusive (29). Changes in nuclear morphology prove to be a useful alternative in this case. Astrakurkurone treatment in our study clearly indicated apoptotic cell death by the appearance of condensed nuclei in DAPI-stained liver cancer cells coupled with enhanced phosphatidylserine externalization and

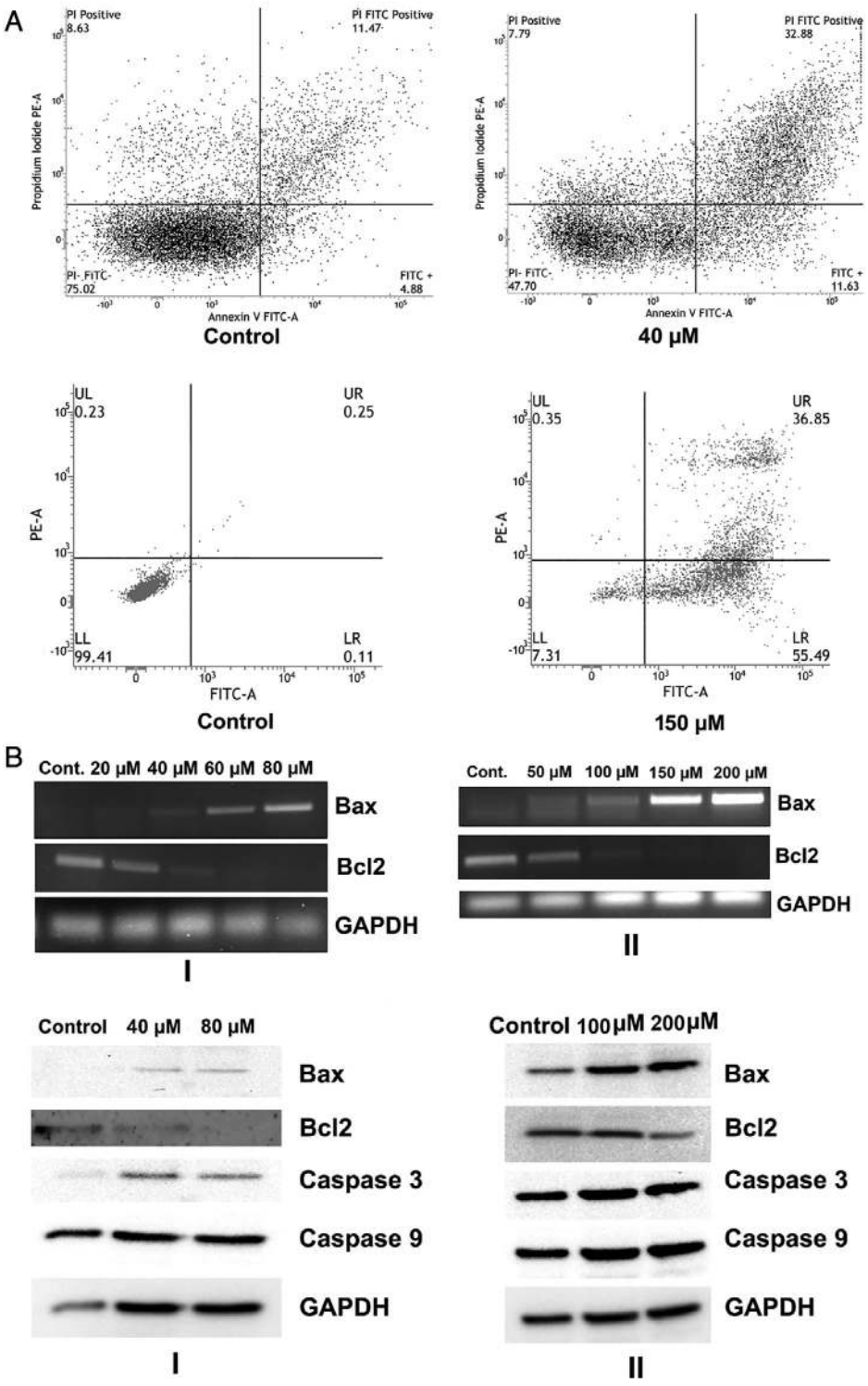

FIG 5

(A) Annexin V-FITC/PI staining and the flow cytometric detection plot from the gated Hep 3B (above) and Hep G2 (below) cells showing populations corresponding to nonapoptotic (Annexin V– PI–), early (Annexin V + PI–), and late (Annexin V+ PI+) apoptotic cells treated with astrakurkurone for 24 h. Data are expressed as mean ± SEM (n = 3), $P < 0.001$. *(B) Comparative gene expression of apoptotic markers from (I) Hep 3B and (II) Hep G2 cells by semiquantitative reverse transcriptase polymerase chain reaction after 24 h of astrakurkurone treatment. GAPDH was used as the loading control. The data represent the best of the replicates (n = 3). (C) Western blot analysis of apoptotic markers from (I) Hep 3B and (II) Hep G2 cells after 24 h of astrakurkurone treatment. GAPDH was used as the loading control. The blot represents the best of the replicates (n = 3).*

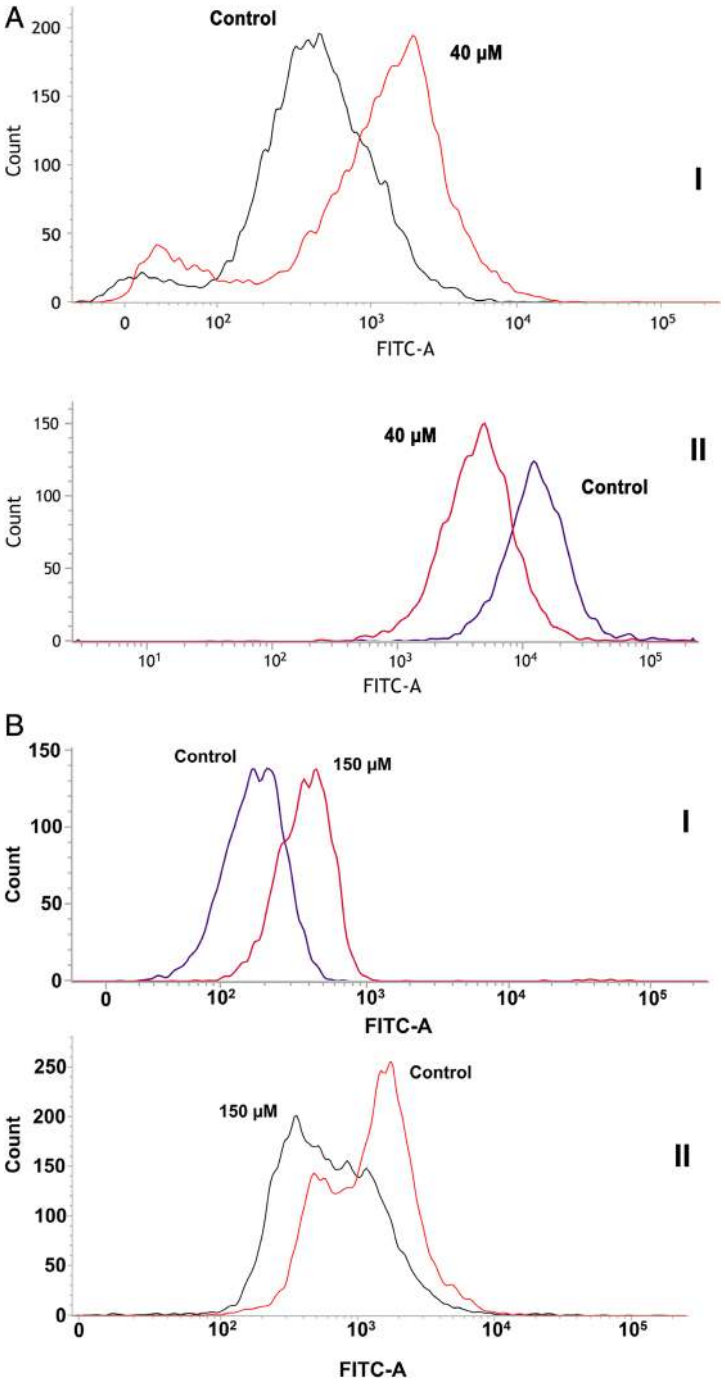

FIG 6 *(A) Flow cytometric analysis showing astrakurkurone-induced (I) ROS generation and (II) depolarization of mitochondrial membrane potential (MMP) in Hep 3B cells after 24 h, (B) flow cytometric analysis showing astrakurkurone-induced (I) ROS generation and (II) depolarization of MMP in Hep G2 cells after 24 h. Data are expressed as mean ± SEM (n = 3),* $P < 0.001$.

plasma membrane permeability as indicated by the quantitative increase of $Annexin^+/PI^+$ cells in flow cytometry.

Diverse chemotherapeutic agents have also been developed that can kill tumor cells by amplifying oxidant stress, by directly generating ROS or inhibiting antioxidant enzymes (30). ROS have been implicated to be involved in tumorigenesis (31), but beyond a threshold, ROS can trigger cellular apoptosis and necrosis (32). Recent studies have also focused on exploring the relation of ROS generation and cancer cell death by natural compounds, like ascorbic acid (33), and on designing ROS-activated anticancer prodrugs as a new strategy for tumor specific damage (30). We have thereby tested the ability of our new drug candidate astrakurkurone in generating intracellular ROS. Astrakurkurone posed to cause potential cellular damage and cell death providing an opportunistic mechanism to kill hepatocellular cancer cells by imposing excessive ROS stress on the malignant cells. Excessive production of ROS may inflict damage to various cellular components including DNA, protein, and lipid membranes (34). Permeabilization of the mitochondrial outer membrane is a potent activator of cell-death initiating pathways. As much of the free radicals are generated in the mitochondria, oxidative stress and mitochondrial damage have been implicated in the pathogenesis of several diseases (35). Damage to the mitochondrial membrane is likely to cause the release of cytochrome *c* and activate the apoptotic cascades (36). Our potential drug candidate astrakurkurone seemed to act in a similar mechanism by depolarizing the mitochondrial membrane, thus utilizing excessive production of ROS and destabilized MMP as two major machineries to target Hep 3B and Hep G2 cells in culture.

Among the significant executors of apoptosis, the caspase family proteins are the fulcrum of the apoptotic cascade. Astrakurkurone treatment indicated an upregulation in the levels of cleaved caspase 3 and caspase 9 of liver cancer cells in a dose-dependent manner. Along with the caspases, several other factors such as the Bcl-2 family proteins also regulate key parts of the apoptotic machinery. The Bcl-2 family comprises both proapoptotic proteins such as Bax, Bak, Bid, Bim, and so on, and prosurvival proteins such as Bcl-2, Bcl-xL, Bcl-w, and so on. These proteins regulate the fate of the cells in a complex series of protein–protein interactions. Astrakurkurone treatment clearly indicated a dose-dependent increase of the proapoptotic marker Bax, along with a concomitant decrease in the anti-apoptotic marker Bcl-2. This altered ratio of Bax/Bcl-2 played the pivotal role in astrakurkurone-induced cell death of Hep 3B/Hep G2 cells.

The balance between cellular proliferation and attrition helps maintain cellular homeostasis and plays an important role in maintaining this homeostasis is the Bcl-2 family of proteins. Among the members that promote apoptosis in the Bcl-2 family, Bax is of profound importance, which in our study was shown to be in an upsurge with astrakurkurone treatment. Bax localized in the cytoplasm translocates into the outer mitochondrial membrane, causing cytochrome *c* release in stressful conditions, which binds with Apaf 1 and caspase 9 to manifest apoptosis (4, 37). The proapoptotic proteins in this family, including Bax, have either three Bcl homology domains or only one Bcl homology domain (BH1–BH3 or only BH3), while prosurvival proteins have four BH

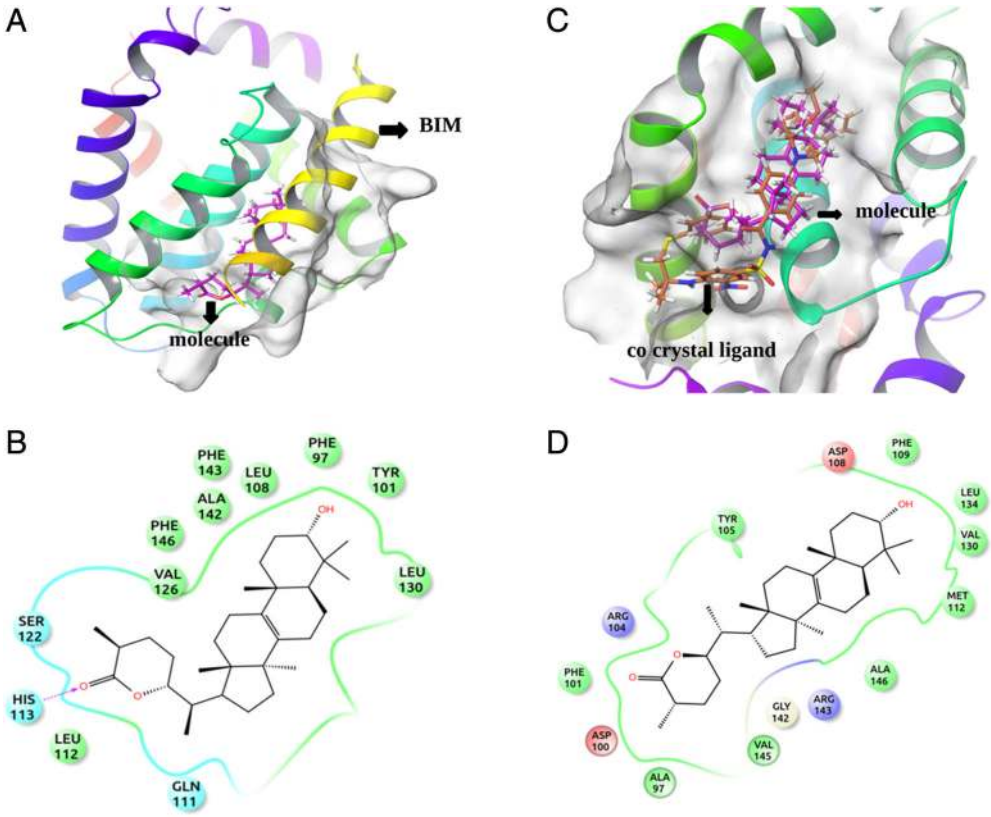

FIG 7 *Detailed interactions between astrakurkurone with Bcl-xL and Bcl-2. (A) Crystal structure of human Bim BH3 helix bound to human Bcl-xL with docked conformation of astrakurkurone (pink stick model) superimposed. (B) Interaction of astrakurkurone with active site residues of Bcl-xL. Hydrogen bonds are shown in pink-dotted lines, and green circle indicates hydrophobic residues and blue indicates positively charged residues. (C) Astrakurkurone-docked conformation (pink stick model) was superimposed with cocrystal ligand (brown stick model) of the crystal structure Bcl-2. (D) Residues of Bcl-2 that interact with astrakurkurone. The green circle residues show the hydrophobic interaction and blue residues show positively charged amino acids.*

domains. These survival promoting proteins manifest their activity by directly binding and segregating their prodeath counterparts (38). Cancer cells can override the apoptotic signals by overexpressing the prosurvival Bcl-2 members (39). Recently, a number of small molecules, including natural and designed, have shown to bind at or near the BH3 domain of prosurvival proteins (38, 40), some of which have also been put to clinical use (41, 42). By binding to the antiapoptotic proteins, the molecules render them unable to sequester the proapoptotic proteins, thus leading the cell toward its death. As evident from our experimental findings, astrakurkurone seemed to disrupt MMP and modulate the Bcl-2 proteins. This led us to investigate whether astrakurkurone possesses any interactive affinity toward Bcl-2 and Bcl-xL. Our study indicated the binding affinity of astrakurkurone to the Bcl-2 family of proteins (Bcl-2 and Bcl-xL), wherein its strong affinity to the BH3 domain may have regulated the core Bcl-2 family proteins to promote apoptosis.

In conclusion, our study has revealed that our proposed drug candidate, astrakurkurone, has potential anticancer activity against HCC cell lines and highlighted on one of its major routes to cellular apoptosis *in vitro*. Further studies would aim to verify the multipotential role of this new drug candidate, involving the triggered downstream signaling pathways, and the identification of some novel molecular targets of the drugs in preclinical cancer models, posing the relevant basis of nurturing its benefits in future clinical trials.

ACKNOWLEDGEMENTS

We are thankful to the Department of Biotechnology, Government of West Bengal, for providing financial support to carry out this research (Grant No. 1261 (sanc)/BT Estt./RD-24/2013).

We would like to thank Pritha Mukherjee for critical reading of the manuscript and Arun Kumar Dutta for helping prepare the figures.

CONFLICT OF INTEREST

The authors declare that they have no conflicts of interest with the contents of this article.

REFERENCES

[1] World Health Organization, Cancer (2017) *SEARO.* [online] http://www.searo.who.int/india/topics/cancer/en/ (Accessed November 29, 2018)

[2] Makin, G., and Dive, C. (2001) Apoptosis and cancer chemotherapy. Trends Cell Biol. 11, S22–S26.

[3] Popgeorgiev, N., Jabbour, L., and Gillet, G. (2018) Subcellular localization and dynamics of the Bcl-2 family of proteins. Front. Cell Dev. Biol. 6, 13.

[4] Gogvadze, V., Orrenius, S., and Zhivotovsky, B. (2006) Multiple pathways of cytochrome c release from mitochondria in apoptosis. Biochim. Biophys. Acta - Bioenerg. 1757, 639–647.

[5] Glasgow, M. D. K., and Chougule, M. B. (2015) Recent developments in active tumor targeted multifunctional nanoparticles for combination chemotherapy in cancer treatment and imaging. J. Biomed. Nanotechnol. 11, 1859–1898.

[6] Iqbal, J., Abbasi, B. A., Mahmood, T., Kanwal, S., Ali, B., et al. (2017) Plant-derived anticancer agents: a green anticancer approach. Asian Pac. J. Trop. Biomed. 7, 1129–1150.

[7] Smith, J. E., Rowan, N. J., and Sullivan, R. (2002) Medicinal mushrooms: a rapidly developing area of biotechnology for cancer therapy and other bioactivities. Biotechnol. Lett. 24, 1839–1845.

[8] Chatterjee, S., Biswas, G., Basu, S. K., and Acharya, K. (2011) Antineoplastic effect of mushrooms: a review. Aus. J. Crop Sci. 5, 904–911.

[9] Standish, L. J., Wenner, C. A., Sweet, E. S., Bridge, C., Nelson, A., et al. (2008) Trametes versicolor mushroom immune therapy in breast cancer. J. Soc. Integr. Oncol. 6, 122–128.

[10] Sullivan, R., Smith, J. E., and Rowan, N. J. (2006) Medicinal mushrooms and cancer therapy. Perspect. Biol. Med. 49, 159–170.

[11] PDQ Integrative, Alternative, and Complementary Therapies Editorial Board, A. and C. T. E. B. (2002) *Medicinal Mushrooms (PDQ®): Patient Version*, National Cancer Institute (US), [online] http://www.ncbi.nlm.nih.gov/pubmed/28267306 (Accessed November 12, 2018)

[12] Biswas, G., Nandi, S., Kuila, D., and Acharya, K. (2017) A comprehensive review on food and medicinal prospects of *Astraeus hygrometricus*. Pharm. J. 9, 799–806.

[13] Lai, T. K., Biswas, G., Chatterjee, S., Dutta, A., Pal, C., et al. (2012) Leishmanicidal and Anticandidal activity of constituents of Indian edible mushroom *Astraeus hygrometricus*. Chem. Biodiersity. 9, 1517–1524.

[14] Mallick, S., Dey, S., Mandal, S., Dutta, A., Mukherjee, D., et al. (2015) A novel triterpene from *Astraeus hygrometricus* induces reactive oxygen species leading to death in Leishmania donovani. Future Microbiol. 10, 763–789.

[15] Mallick, S., Dutta, A., Chaudhuri, A., Mukherjee, D., Dey, S., et al. (2016) Successful therapy of murine visceral Leishmaniasis with Astrakurkurone, a Triterpene isolated from the mushroom *Astraeus hygrometricus*, involves the induction of protective cell-mediated immunity and TLR9. Antimicrob. Agents Chemother. 60, 2696–2708.

[16] FRAMBO v. 4.1.05 "Program for Data Collection on Area Detectors" BRUKER-Nonius Inc., 5465 East Cheryl Parkway, Madison, WI 53711-5373 USA

[17] APEX2 "Program for Data Collection and Integration on Area Detectors" BRUKER AXS Inc., 5465 East Cheryl Parkway, Madison, WI 53711-5373 USA

[18] Sheldrick, G. M. (2008) SADABS, Programs for Scaling and Absorption Correction of Area Detector Data. *SADABS, Programs Scaling Absorpt. Correct. Area Detect. Data*

[19] Dolomanov, O. V., Bourhis, L. J., Gildea, R. J., Howard, J. A. K., and Puschmann, H. J. (2009) OLEX2: a complete structure solution, refinement and general all round good thing Olex2. J. Appl. Cryst. 42, 339–341.

[20] Sheldrick, G. M. "Cell_Now (version 2008/1): Program for Obtaining Unit Cell Constants from Single Crystal Data": University of Göttingen, Germany

[21] Tate, E. H., Wilder, M. E., Cram, L. S., and Wharton, W. (1983) A method for staining 3T3 cell nuclei with propidium iodide in hypotonic solution. Cytometry 4, 211–215.

[22] Chang, H.-Y., Huang, H.-C., Huang, T.-C., Yang, P.-C., Wang, Y.-C., et al. (2013) Flow Cytometric detection of mitochondrial membrane potential. Bio-Protocol. e430. https://doi.org/10.21769/BioProtoc.430.

[23] Maeda, H., and Khatami, M. (2018) Analyses of repeated failures in cancer therapy for solid tumors: poor tumor-selective drug delivery, low therapeutic efficacy and unsustainable costs. Clin. Transl. Med. 7, 11.

[24] Tsuchiya, N., Sawada, Y., Endo, I., Uemura, Y., and Nakatsura, T. (2015) Potentiality of immunotherapy against hepatocellular carcinoma. World J. Gastroenterol. 21, 10314–10326.

[25] Blagodatski, A., Yatsunskaya, M., Mikhailova, V., Tiasto, V., Kagansky, A., et al. (2018) Medicinal mushrooms as an attractive new source of natural compounds for future cancer therapy. Oncotarget 9, 29259–29274.

[26] Ye, M., Liu, J., Lu, Z., Zhao, Y., Liu, S., et al. (2005) Grifolin, a potential antitumor natural product from the mushroom *Albatrellus confluens*, inhibits tumor cell growth by inducing apoptosis in vitro. FEBS Lett. 579, 3437–3443.

[27] Fulda, S., Galluzzi, L., and Kroemer, G. (2010) Targeting mitochondria for cancer therapy. Nat. Rev. Drug Discov. 9, 447–464.

[28] Cummings, B. S., Schnellmann, R. G., and Schnellmann, R. G. (2004) Measurement of cell death in mammalian cells. *Curr. Protoc. Pharmacol.* Chapter 12, Unit 12.8

[29] Kamalidehghan, B., Ahmadipour, F., and Noordin, M. I. (2012) DNA fragmentation is not associated with apoptosis in zerumbone-induced HepG2 cells. Iran. Biomed. J. 16, 226.

[30] Peng, X., and Gandhi, V. (2012) ROS-activated anticancer prodrugs: a new strategy for tumor-specific damage. Ther. Deliv. 3, 823–833.

[31] Ray, P. D., Huang, B.-W., and Tsuji, Y. (2012) Reactive oxygen species (ROS) homeostasis and redox regulation in cellular signaling. Cell. Signal. 24, 981–990.

[32] Dharmaraja, A. T. (2017) Role of reactive oxygen species (ROS) in therapeutics and drug resistance in cancer and bacteria. J. Med. Chem. 60, 3221–3240.

[33] Molavian, H. R., Goldman, A., Phipps, C. J., Kohandel, M., Wouters, B. G., et al. (2016) Drug-induced reactive oxygen species (ROS) rely on cell membrane properties to exert anticancer effects. Sci. Rep. 6, 27439.

[34] Hensley, K., Robinson, K. A., Gabbita, S. P., Salsman, S., and Floyd, R. A. (2000) Reactive oxygen species, cell signaling, and cell injury. Free Radic. Biol. Med. 28, 1456–1462.

[35] Guo, C., Sun, L., Chen, X., and Zhang, D. (2013) Oxidative stress, mitochondrial damage and neurodegenerative diseases. Neural Regen. Res. 8, 2003–2014.

[36] Pelicano, H., Feng, L., Zhou, Y., Carew, J. S., Hileman, E. O., et al. (2003) Inhibition of mitochondrial respiration. J. Biol. Chem. 278, 37832–37839.

[37] Wolter, K. G., Hsu, Y. T., Smith, C. L., Nechushtan, A., Xi, X. G., et al. (1997) Movement of Bax from the cytosol to mitochondria during apoptosis. J. Cell Biol. 139, 1281–1292.

[38] Bruncko, M., Oost, T. K., Belli, B. A., Ding, H., Joseph, M. K., et al. (2007) Studies leading to potent, dual inhibitors of Bcl-2 and Bcl-xL. J. Med. Chem. 50, 641–662.

[39] Green, D. R., and Evan, G. I. (2002) A matter of life and death. Cancer Cell 1, 19–30.

[40] Wei, J., Kitada, S., Stebbins, J. L., Placzek, W., Zhai, D., et al. (2010) Synthesis and biological evaluation of Apogossypolone derivatives as pan-active inhibitors of Antiapoptotic B-cell lymphoma/Leukemia-2 (Bcl-2) family proteins. J. Med. Chem. 53, 8000–8011.

[41] Souers, A. J., Leverson, J. D., Boghaert, E. R., Ackler, S. L., Catron, N. D., et al. (2013) ABT-199, a potent and selective BCL-2 inhibitor, achieves antitumor activity while sparing platelets. Nat. Med. 19, 202–208.

[42] van Delft, M. F., Wei, A. H., Mason, K. D., Vandenberg, C. J., Chen, L., et al. (2006) The BH3 mimetic ABT-737 targets selective Bcl-2 proteins and efficiently induces apoptosis via Bak/Bax if Mcl-1 is neutralized. Cancer Cell 10, 389–399.